Multi-approach characterization of shallow-water carbonates off Minamitorishima and their depositional settings/history

[1]MD. AFTABUZZAMAN, [1]KAZUKI YOMOGODA, [1]SHOTA SUZUKI, [1]HIDEKO TAKAYANGI, [1]AKIMASA ISHIGAKI, [2]SHIKI MACHIDA, [3]YOSHIHIRO ASAHARA, [3]KOSHI YAMAMOTO, [4]NAOTO HIRANO, [5]SHIN-ICHI SANO, [6]SHUN CHIYONOBU, [7]DAVIDE BASSI, [1]*YASUFUMI IRYU

[1] *Institute of Geology and Paleontology, Graduate School of Science, Tohoku University, Aramaki-aza-aoba 6-3, Aoba-ku, Sendai 980-8578, Japan,* [2] *Ocean Resources Research Center for Next Generation, Chiba Institute of Technology, 2-17-1 Tsudanuma, Narashino, Chiba, 275-0016, Japan,* [3]*Department of Earth and Environmental Sciences, Graduate School of Environmental Studies, Nagoya University, Furo-cho, Chikusa-ku, Nagoya 464-8601, Japan,* [4]*Center for Northeast Asian Studies, Tohoku University, Kawauchi 41, Aoba-ku, Sendai 980-8576, Japan,* [5] *Department of Earth System Science, School of Sustainable Design, University of Toyama, Gofuku, Toyama 930-8555, Japan*, [6]*Department of Earth Resource Science, Faculty of International Resource Sciences, Akita University, 1-1 Tegata-Gakuencho, Akita 010-8502, Japan,* [7] *Dipartimento di Fisica e Scienze della Terra, Università degli Studi di Ferrara, I-44122 Ferrara, Italy.*

*** Correspondence**

Yasufumi Iryu, Institute of Geology and Paleontology, Graduate School of Science, Tohoku University, Aramaki-aza-aoba 6-3, Aoba-ku, Sendai 980-8578, Japan.

Tel: +81 227956622; Fax: +81 227956634

yasufumi.iryu.d8@tohoku.ac.jp

ORCID

Yasufumi Iryu: https://orcid.org/0000-0002-6099-0662

Authors' email addresses

Md. Aftabuzzaman： aftabuzzaman.mohammad.s8@dc.tohoku.ac.jp

Kazuki Yomogida： kazuki1020619@gmail.com

Shota Suzuki: bosssaboten@gmail.com

Hideko Takayanagi: hideko.takayanagi.b4@tohoku.ac.jp

Akimasa Ishigaki: akimasa.ishigaki.q1@dc.tohoku.ac.jp

Shiki Machida: shiki.machida@p.chibakoudai.jp

Yoshihiro Asahara: asahara@eps.nagoya-u.ac.jp

Koshi Yamamoto: hamchans@nagoya-u.jp

Naoto Hirano: nhirano@tohoku.ac.jp

Shin-ichi Sano: ssano@sus.u-toyama.ac.jp

Shun Chiyonobu: chiyo@gipc.akita-u.ac.jp

Davide Bassi: bsd@unife.it

Yasufumi Iryu: yasufumi.iryu.d8@tohoku.ac.jp

Conflict of interest

The authors have no competing interests to declare.

Availability of data and materials

Please contact the corresponding author regarding data requests.

Abstract

Sedimentological, geochemical, and chronological analyses were carried out on 19 carbonate rock samples collected from the submarine slope to the west of Minamitorishima (Marcus Island) located near the western margin of the Pacific Plate. Four groups of carbonate rocks were distinguished: mollusk-rich carbonates, coral-rich carbonates, foraminiferal-nannofossil packstone, and mudstone/wackestone. The mollusk-rich carbonates are characterized by dominance of bivalve (including rudist) and gastropod shells. Skeletal grains are extensively bioeroded, some with thick micrite envelopes. Sr isotope ratios ($^{87}Sr/^{86}Sr$) and *Mesorbitolina* ex gr. *texana* (large benthic foraminifer) indicate that the shallow-water carbonates were deposited in the late Aptian–early Albian (~122–111 Ma). The coral-rich carbonates are characterized by abundant scleractinian corals and nongeniculate coralline algae associated with encrusting acervulinid foraminifers. The biotic composition indicates that the carbonates were deposited in a coral reef setting during the Oligocene–Miocene. Geochemical data show that the coral-rich carbonate were dolomitized at 6.8–9.5 Ma (Tortonian–Messinian) and that normal seawater is the likely parent fluid. The foraminiferal-nannofossil packstone is semi-consolidated foraminiferal-nannofossil ooze, deposited in the Pleistocene (0.99–0.45 Ma). The mudstone/wackestone is marked by absence of macrofossils and is phosphatized: its age and depositional environment could not be assessed. The Cretaceous mollusk-rich carbonates are distributed to shallower depths than expected following standard seafloor subsidence, clearly showing that Minamitorishima has undergone not continuous thermal subsidence but significant episodic uplifts probably by Eocene volcanism.

Key words: Cretaceous, Dolomite, Minamitorishima (Marcus Island), Miocene, Oligocene, Orbitolinid large benthic foraminifer, Rudist, Shallow-water carbonate, Sr isotope.

Running head: Carbonate rocks off Minamitorishima

1. INTRODUCTION

Minamitorishima (Marcus Island) is a carbonate island located ~1150 km to the east of the Izu-Ogasawara Trench, the boundary between the Pacific and Philippine Sea plates (Figure 1a). This area, near the western margin of the Pacific Plate (24°17'N; 153°59'E), represents an older portion of the Pacific Plate. Formed during the Early to Late Cretaceous, the numerous seamounts occurring on this older portion, including Minamitorishima (Marcus Island), are collectively called the Western Pacific Seamount Province (WPSP; Sager et al., 1993; Koppers et al., 2003).

Because Minamitorishima is an emerged carbonate island on the old volcanic edifice, it is likely that reef and carbonate platform deposits formed in the Cretaceous onwards occur subsurface. For this reason, this island has been selected as one of sixteen "proposed continental scientific drilling sites in Japan" in the 1980s (Niitsuma, 2003). After the selection, however, no research has been carried out on these carbonate deposits aiming to a continental scientific drilling.

In the northwestern Pacific Ocean many seamounts are commonly covered with shallow-water carbonate deposits. Based on lithological and chronological analyses of Cretaceous to Pleistocene shallow-water carbonates collected from 29 sites on 24 submerged seamounts, Takayanagi et al. (2007, 2012) showed that the timing of deposition of those shallow-water carbonates might not have been controlled by climatic conditions. Rather the timing was predominantly related to the volcanism and tectonics that served as the basement for reef/carbonate-platform formation. Therefore, the Minamitorishima carbonates are expected to be an excellent database for the reef/carbonate platform evolution and related ecosystems for the last 100 Myr or more and the climate and tectonics control on the buildup and its biotic/abiotic components.

We performed sedimentological and chronological analyses of carbonate rocks collected in the western Minamitorishima (Table 1). After distinguishing four groups of carbonate rocks, each of which was deposited/dolomitized/phosphatized at different timing, we discuss their depositional history.

2. GEOLOGIC SETTING

The oceanic crust around Minamitorishima is 160–150 Ma in age (Koppers et al., 2003). This is younger than the Jurassic Quiet Zone (> 160 Ma; Handschumacher et al., 1988; Tivey et al., 2006) located immediately to the east/southeast of this island.

On the present western Pacific Plate, most seamounts, islands and atolls were formed during the Cretaceous submarine intra-plate volcanism (e.g., Tokuyama, 1980; Larson, 1991; Haggerty & Silva, 1995). As a consequence, there are several seamount chains or hot spot trails (Koppers et al., 2003) in the WPSP. Minamitorishima, together with Wake atoll and many guyots, constitutes the Marcus-Wake Seamounts (Smoot, 1989). No island exists around Minamitorishima, where many seamounts are known to occur. The nearest Wake Island is located ~1400 km to the east-southeast of Minamitorishima. Consequently, the question gets arisen why only Mimamitorishima exists as an island. But this remains unsolved.

Minamitorishima is triangular with a side of ~2 km in shape (apex to the north, south and west) (Figure 1b). The area of the island is 1.51 km^2 and the maximum elevation is 9 m. It had been interpreted as a typical elevated atoll in the Central Pacific because of its geomorphologic similarity to modern atolls (Bryan, 1903): the occurrence of a topographic depression comparable to a past lagoon in the center of the island, six benchlike steps correlative to uplifted marine terraces, and an exposed or elevated reef at an elevation of ~2 m. The maximum elevation was reported to reach ~23 m. However, the interpretation that Minamitorishima is a typical elevated atoll was denied by Konishi et al. (1985). They showed two lines of negative evidence indicating almost no tectonic uplift of Minamitorishima: the highest elevation is only 9 m and that the carbonate deposits, interpreted as an exposed reef, in the northeastern part of this island are actually beach conglomerate formed at a relatively high sea-stand period in the Late Holocene (~2.4–3.2 ka). No study has been conducted on carbonate deposits in the subsurface of and on the submarine slope of Minamitorishima.

3 MATERIALS AND METHODS

3.1 Materials

We examined carbonate samples collected from the submarine slope to the west of Minamitorishima (Figure 1b, Table 1) by the submersible *Shinkai 6500* during the scientific cruise of *R/V Yokosuka* (YK10-05 and YK17-11C) of the Japan Agency for Marine-Earth Science and Technology. The samples were collected at three water depths: 938 m, 1085 m, and 3354 m.

3.2 Methods

3.2.1 Core description

Because the all samples, except for YK10-05 6K#1209 R-05, are coated naturally with manganese (oxyhydr)oxides, they are cut into several slabs to visually observe components and texture of the collected carbonates. Subsequently, thin sections were prepared and examined to identify carbonate microfacies. Classification of carbonate rocks basically follows Dunham (1962) and Embry and Klovan (1971). Terms for larger foraminiferal shell structures and architectures are those used by Hottinger (2006).

3.2.2 X-ray diffraction analysis

Before Sr isotope measurements were made, mineral abundance of bulk-rock carbonate samples was determined by X-ray diffraction (XRD) analyses, following Suzuki et al. (2006). Mineral abundance was determined by XRD analyses of randomly orientated powders on a Phillips X'pert-MPD PW3050 system at the Institute of Geology and Paleontology, Graduate School of Science, Tohoku University (IGPS), using Cu Kα radiation. Sideloaded samples were scanned between 208 and 6082h with a step size 0.0282h and a counting time of 0.5 s/step. Following Cook et al. (1975), mineral weight percentages were calculated by the integrated peak intensity.

3.2 Sr isotope analysis

To provide chronological constraints on the studied carbonates, Sr isotope ratios ($^{87}Sr/^{86}Sr$) were analyzed for 15 samples. The $^{87}Sr/^{86}Sr$ values were measured with thermal ionization mass spectrometers (VG Sector 54-30 and GVI IsoProbe-T) at the Department of Earth and Environmental Sciences, Nagoya University, following protocols by Asahara et al. (1999, 2006) and Suzuki et al. (2012). Replicate analyses of the National Institute of Standards and Technology (NIST) Standard Reference Material 987 during this study gave values of 0.710259±0.000022 (2σ, n = 7, October 2018) and 0.710279±0.000025 (2σ, n = 7, July 2020). All measurements were normalized to 0.710248 (McArthur et al. 2001). Numerical ages were determined by a comparison between the obtained $^{87}Sr/^{86}Sr$ values and the global calibration curve proposed by McArthur et al. (2012). The geologic time scale of Gradstein et al. (2012) was referred to.

3.3 Stable carbon and oxygen isotope and trace element analyses of dolomite samples

We conducted analyses of isotopic and geochemical composition of dolomites off Minamitorishima to reveal the origin of these dolomites. Stable carbon and oxygen isotope analysis of dolomite powder samples was performed using a Thermo Fisher Delta V Advantage isotope ratio mass spectrometer coupled to a Gasbench II automated carbonate preparation device, at the IGPS. The samples (~ 0.2 mg) were reacted with 100% phosphoric acid at ~60 °C. The isotope ratios were expressed in conventional (δ‰) notation and calibrated to the NBS-19 international standard relative to the Vienna Pee Dee Belemnite (VPDB). The external precision (1σ) based on replicate measurements (n = 55) of the laboratory reference material (dolomite sample 18-1 from Kita-daito-jima, Suzuki et al., 2006, figure 14; JCp-1, Okai et al., 2004; NBS-19; CO-1) was 0.01‰ for the carbon isotope analysis and 0.09‰ for oxygen isotope analysis.

Powdered dolomite samples (500 μg) were dissolved in ~ 5.6 mL of volume-specific 2% (v/v) nitric acid (HNO_3). Concentrations of the three minor elements (Mn, Fe, Sr) were analyzed using an Agilent 7700x inductively coupled plasma mass spectrometer at the Department of Earth and Environmental Sciences, Nagoya University, Japan. Minor elemental concentrations are expressed as ppm (= μg/g). The precision of the analytical method, expressed as the relative standard deviation (σ) of repeated analyses of the laboratory reference material (JCt-1; Okai et al. 2004), was less than 10% for the all elements.

3.4 Calcareous nannofossil biostratigraphy

Samples were prepared for calcareous nannofossil analysis using standard smear slide methods and optical adhesive as a routing medium (Bown & Young , 1998). Calcareous nannofossils were analyzed under an optical polarizing microscope at 1500x magnification.

4 RESULTS

4.1 Lithology

Based on their lithology and ages of deposition and dolomitization, four carbonate groups were distinguished: (1) mollusk-rich carbonates (Figure 2), (2) coral-rich carbonates (Figure 3), (3) Pleistocene foraminiferal-nannofossil packstone (Figure 4), (4) mudstone/wackestone (Figure 5). These groups were composed exclusively of calcite, dolomite, apatite, and calcite, respectively.

4.1.1 Mollusk-rich carbonates

YK17-11C 6K#1502 N4-001: Molluscan floatstone with chondrodont bivalves

This white- to beige-colored floatstone, with bioclastic grainstone matrix, characteristically contained chondrodont bivalves (Figures 2a and 6a). Other bivalves (including rudists) and gastropods were common. A relatively large nerineoid gastropod (about 3 cm in shell width) also occurred. The molluscan shells were extensively bioeroded. A few bivalve shells were encrusted by microbial filaments. The bioclasts of the grainstone matrix were dominated by medium to coarse sand-sized molluscan shells, mostly with micrite envelopes. The shells were commonly replaced partly to completely with sparry cements. Other bioclasts, including echinoids and solenoporacean algae, were rare. Large benthic foraminifers were represented by orbitolinids (*Mesorbitolina*?). Intraclasts constituted a subordinate component. Moldic porosity and dissolution vugs were common: their walls were fringed by sparry cements. Intergranular pore space was partly to completely filled with isopachous bladed and equant mosaic cements.

YK17-11C 6K#1502 N5-005: Molluscan floatstone

This white- to beige-colored floatstone was characterized by the occurrence of up to pebble-sized bivalves (including rudists) and gastropods associated with corals (Figures 2b and 6b). Some of the gravel-sized bioclasts were encrusted by microbialites and encrusting foraminifers. The grainstone matrix consisted mainly of fine to medium sand-sized bioclasts of bivalves, gastropods, and intraclasts. *Mesorbitolina* cf. *birmanica* (Sahni, 1937) commonly occurred. Echinoids and nongeniculate coralline algae are subordinate. The rudists shells were extensively bioeroded. The bioclasts mostly had micrite envelopes. Intraclasts were common. Moldic porosity and dissolution vugs commonly occurred. Intergranular pore space was partly to completely filled with isopachous bladed and quant mosaic cements.

YK17-11C 6K#1502 N5-006: Intraclastic-bioclastic rudstone

This rudstone was beige to pale reddish beige in color and indurated at the relatively well preserved part (Figure 2c). In contrast, altered part was white and vulnerable. The rudstone was characterized by abundant occurrence of very coarse sand- and granule-sized skeletal and non-skeletal grains, having a relatively coarse appearance (Figure 6c).

Pebble-sized grains were rare. The grains were dominated by bioclasts of molluscan shells (probably mostly bivalve shells) and intraclasts. Subordinate bioclasts included corals, solenoporacean algae, and echinoids. Some bivalve shells were bioeroded. The bioclasts mostly had micrite envelopes. Poorly preserved nannofossils (*Discoaster* spp., *Reticulofenestra* sp.) were also present. Rare moldic porosity and dissolution vugs occurred. The inner space in a rudist shell was filled with an internal sediment and unconsolidated lime mud (Figure 2c). The grains were fringed by two generations of isopachous cements (bladed cements succeeded by dog-tooth cements). The secondary isopachous cements were succeeded by coarse equant mosaic cements.

YK17-11C 6K#1502 N5-008: Molluscan floatstone

This beige-colored rudstone was characterized by containing abundant up to pebble-sized gastropods (Figure 2d). Rudists were rarely found. The matrix consisted of packstone and grainstone dominated by bioclasts of molluscan shells and intraclasts (Figure 6d). The shells were commonly replaced partly to completely with sparry cements. Other bioclasts were derived from echinoids, coralline and solenoporacean algae, and planktic foraminifers. The bioclasts mostly had micrite envelopes. Moldic porosity and dissolution vugs were common. Intergranular pore space was filled with peloidal micrite or two generations of isopachous cements and coarse equant mosaic cements just like the cements in sample YK17-11C 6K#1502 N5-006.

YK17-11C 6K#1502 N5-010: Carbonate crusts and bioclastic packstone

This beige-colored limestone was composed of carbonate crusts and bioclastic packstone (Figure 2e). The crusts, up to 6 mm thick, consisted mainly of micrite with many domal to irregularly-shaped vacant spaces that were up to 1 mm across and up to 400 μm high (Figure 6e). The crust walls partly seemed to be microfibrous. The genesis of these crusts was uncertain. The bioclastic packstone consisted mainly of thin shelled bivalves, gastropods, and large benthic foraminifers (*Mesorbitolina* ex gr. *texana* (Roemer 1849)). Many shells were replaced with sparry cements. The bioclasts had micrite envelopes; cortoids occurred as a minor component. Abundant dissolution vugs filled with peloids (peloidal aggregates) and sparry calcite occurred.

YK17-11C 6K#1502 N5-011: Bioclastic grainstone

This beige- to whitish-beige-colored grainstone was composed mostly of up to granule-sized bioclasts of mollusks (mainly bivalves) (Figures 2f, 6f). Other bioclasts, included echinoids and large benthic foraminifers (*Mesorbitolina*?) were rare. Intraclast constituted a minor component. Most of the bioclasts had micrite envelopes. The mollusk shells were commonly replaced partly to completely with sparry cements. Dissolution vugs were common. Planktic foraminifers were found in some dissolution vugs. Intergranular pore space was partly to completely filled with two generations of isopachous cements spaces and coarse equant mosaic cements.

YK17-11C 6K#1502 N5-014: Molluscan rudstone

This beige-colored rudstone was composed mainly of granule- to pebble-sized bioclasts of mollusks (dominated by bivalves) and, to a lesser extent, corals and echinoids (Figures 2g, 6g). The space among these gravel-sized bioclasts was filled with bioclastic packstone/wackestone or sparry cements. The packstone/wackestone was composed of the same bioclasts as the gravel-sized ones: the intergranular space is filled with partly peloidal micrite. The bioclasts were mostly had micrite envelopes. Moldic porosity and dissolution vugs were rare. The sparry cements showed a succession that started with greyish bladed cements fringing bioclasts, which was succeeded by dog-tooth cements and, in turn, coarse equant mosaic cements.

4.1.2 Coral-rich carbonates

YK17-11C 6K#1502 N5-001: Coral rudstone

Although it was completely dolomitized, the original fabric of this white- to light-beige-colored rudstone was not completely destroyed (fabric-preserving dolomite; Figures 3a, 7a). Corals were up to boulder sized, mostly massive, and covered with nongeniculate coralline algae and encrusting foraminifers. The matrix was likely to be grainstone composed of bioclasts of corals, mollusks, echinoids, benthic foraminifers (including encrusting acervulinid foraminifers), and possible bryozoans. Many of the bioclasts were replaced with dolomite crystals. Micrite filling the intergranular space was dolomitized and coarsened. Intraskeletal pore space in the corals was filled with micrite with very fine sand-sized bioclasts and/or silt-sized micrite grains.

YK17-11C 6K#1502 N5-002: Fossil coral

This light-beige-colored sample consisted exclusively of a massive agariciid coral (Figure 3b). Although coral skeletal structure was preserved, the skeleton was replaced with dolomite crystals (Figure 7b). Intraskeletal pore space within the coral was filled partly to completely with dolomite crystals or coarsened micrite rarely with bioclasts of nongeniculate coralline algae and bivalves.

YK17-11C 6K#1502 N5-004: Coral floatstone

This beige-colored floatstone characteristically contained abundant fragments of coral branches (0.5–1.3 cm in mean diameter; Figure 3c). A massive coral (8 cm across) occurs. The corals were encrusted by acervulinid foraminifers. Although this floatstone was completely dolomitized, its original fabric was well preserved (Figure 7c). The matrix consisted of packstone dominated by bioclasts of corals, dasycladalean algae, geniculate and nongeniculate coralline algae, bivalves, and gastropods. Intergranular pore space was filled with micrite. Dissolution vugs were fringed with at least five generations of cements, two of which were light brown to beige in color.

YK17-11C 6K#1502 N5-007: Bioclastic grainstone with corals

This white-colored grainstone contained coral fragments (Figure 3d). The corals were limited in number occurrence and amount, including a thickly branching (2.7 cm across and > 3 cm long) colony and a massive colony (~ 13 cm across, ~ 11 cm high). Nongeniculate coralline algae are abundant in this grainstone (Figure 7d). Bivalves, benthic foraminifers, and echinoids were subordinate. This is due to selective preservation of coralline algae. It is likely that more bioclasts were initially contained and that many of them were dissolved and replaced with dolomite crystals. Intergranular pore space was filled with dolomite cements.

YK17-11C 6K#1502 N5-009: Coral floatstone

This sample is similar in color, fabric, and biotic composition to the sample YK17-11C 6K#1502 N5-004. This beige-colored floatstone was characterized by abundant fragments of coral branches that were up to 2 cm across (Figures 3e, 7e). Some of the corals were encrusted by acervulinid foraminifers or nongeniculate coralline algae (Figure 7f). The original fabric of this floatstone was well preserved. The matrix was packstone composed mainly of bioclasts of corals, nongeniculate coralline algae, mollusks (bivalves being more common), dasycladalean algae and benthic foraminifers. Echinoids and bryozoans occur as a minor component. Dissolution vugs were fringed with multiple generations of cements.

YK17-11C 6K#1502 N5-012: Fossil coral

This light-beige-colored sample was composed solely of a massive coral, whose skeletal structure was mostly destroyed and replaced with dolomite crystals (Figure 3f).

YK17-11C 6K#1502 N5-013: Coral floatstone

This light-beige- to white-colored floatstone, with bioclastic packstone matrix, contained fragments of massive corals (Figure 3g). The largest colony size is ~ 3 cm across and ~ 11 cm high on the polished slab. The bioclasts were dominated by nongeniculate coralline algae due to the selective preservation as in YK17-11C 6K#1502 N5-007 (Figure 7g). Bivalves were subordinate. The intergranular pore space was mostly filled with dolomite microspars replacing micrite, which locally occurred in intraskeletal pore space.

YK17-11C 6K#1502 N5-015: Fossil coral

This sample consisted of a beige fragment of a massive coral (Figure 3h). The original skeletal structure of this coral was relatively well preserved although its skeleton was replaced with dolomite crystals (Figure 7h). Some corallites were encrusted by acervulinid foraminifers. Inter- and intraskeletal pore space was filled partly with up to coarse sand-sized bioclasts and micrite, showing a packstone texture.

4.1.3 Foraminiferal-nannofossil packstone

YK10-05 6K#1209 R-05: Foraminiferal-nannofossil packstone

This white-colored semi-consolidated packstone was without manganese coating (Figure 4) and consisted exclusively of planktic foraminifers and calcareous nannofossils (consolidated foraminiferal-nannofossil ooze). These were represented by *Gephyrocapsa parallela* Hay & Beaudry, 1973 and *Pseudoemiliania lacunose* Kamptner, 1963 ex Gartner, 1969. No diagenetic products were identified.

4.1.4 Mudstone and wackestone

YK17-11C 6K#1502 N4-002: Mudstone

This mudstone consisted of multiple generations of phosphatized mudstones: i.e., light brown-colored, weakly laminated mudstone, cream- to light brown-colored, porous mudstone, and light brown internal sediment (Figures 5a, 8a). However, the former two could not be clearly distinguished, grading into each other. Biogenics (e.g., mollusks) were rarely found. Possible moldic porosity due to dissolution of planktic foraminifers rarely occurred.

YK17-11C 6K#1502 N5-003: Wackestone and mudstone

This phosphatized sample was composed of two lithologies: light brown-colored laminated bioclastic wackestone and dark brown-colored, partly laminated mudstone, both with bioturbated micritic matrix (Figure 5b). The former was characterized by abundant, possible molds of microfossils, most of them were dissolved to leave moldic porosity (Figure 8b). The bioclasts of planktic foraminifers, ostracods, and echinoid spines were rarely found. The partly laminated mudstone differs from the bioclastic wackestone in containing less possible molds of microfossils.

4.2 Dolomite geochemistry

$\delta^{13}C$ and $\delta^{18}O$ values of the Minamitorishima fell in a range from 3.64 to 4.07 ‰ and from 1.50 to 1.88 ‰, respectively (Table 2). Sr, Fe, and Mn concentrations fell in ranges of 27–34 ppm (with one outlier of 120 ppm), 170–190 ppm, and 200–250 ppm, respectively.

4.3 Chronology

The $^{87}Sr/^{86}Sr$ reference curve for Cretaceous seawater (McArthur et al., 2012; age derived using the look-up table, LOWESS 5 Fit 26 03 13) decreases simply from the Maastrichtian to the Campanian and fluctuates from the Santonian to the Berriasian. Thus, $^{87}Sr/^{86}Sr$ values of carbonates formed in the former period yield uniquely one age. Whereas plural ages may be assigned for $^{87}Sr/^{86}Sr$ values of those formed in the latter period. Actually, numerical ages of the all studied carbonate samples could not be uniquely determined (Table 3) and fell into a wide range from 140.4 Ma (Berriasian) to 87.9 Ma (Coniacian). However, the occurrence of an age-diagnotic large benthic foraminifer, *Mesorbitolina* ex gr. *texana* (Schroeder et al., 2010), the studied shallow-water carbonates are dated as late Aptian–early Albian (~123–111 Ma; see 5.1.2 orbitolinid foraminifer).

$^{87}Sr/^{86}Sr$ values of dolomites have been used to date the dolomitization. In case that the sources of Sr are limited to the original sediments and the dolomitizing fluids are seawater of a later age, Sr isotope signature records the oldest possible age of dolomitization (Swart et al., 1987; Vahrenkamp et al., 1991). The studied coral-rich carbonates had the $^{87}Sr/^{86}Sr$ values assignable to 6.8–9.5 Ma (8.5 ± 0.9 Ma; Tortonian to Messinian). Because neither precursor calcite nor aragonite was contained in the coral-rich carbonates, the Sr isotope ages indicate the timing of dolomitization. The depositional age (Oligocene–Miocene) of the coral-rich carbonates is discussed in "5.1 Biotic composition".

Gephyrocapsa parallela and *Pseudoemiliania lacunose* whose first and last occurrences define the datums 6 (0.99 Ma) and 3 (0.45 Ma) of Sato et al. (2009), respectively, were detected from the foraminiferal-nannofossil packstone sample (YK10-05 6K#1209 R-05). Therefore, this packstone is deposited during the period of 0.99–0.45 Ma. The unconsolidated internal sediment in the sample YK17-11C 6K#1502 N5-006 yielded poorly preserved nannofossils (*Discoaster* spp. and *Reticulofenestra* sp.), possibly suggesting a Pleistocene age (< 1.99 Ma; Sato et al., 2009).

Neither depositional nor phosphatization age could be constrained in this study.

5. DISCUSSION

5.1 Biotic composition

The shallow-water carbonates collected off Minamitorishima are grouped into mollusk-rich carbonates and coral-rich carbonates. The mollusk-rich carbonates are characterized by abundant mollusks (including rudists) and common bioeroded bioclasts, many of which possess thick micrite envelopes. Whereas, the coral-rich carbonates are dominated by scleractinian corals and nongeniculate coralline algae, commonly associated with encrusting acervulinid foraminifers. This contrast agrees with that reported in previous studies (Iryu & Yamada, 1999; Perrin, 2002; Kiessling, 2009; Takayanagi et al., 2012). Based on sedimentological and chronological analysis of Cretaceous to Pleistocene shallow-water carbonates collected from submerged seamounts in the northwestern Pacific, Takayanagi et al. (2012) show that those carbonates can be classified into three types, C-type, E-type, and OP-type formed in the Cretaceous, Eocene (probably including earliest Oligocene), and Oligocene to Pleistocene, respectively. The mollusk-rich carbonates and the coral-rich carbonates off Minamitorishima are identical to C-type and OP-type, respectively. The compositional differences of C-type and OP-type shallow-water carbonates have been interpreted to reflect a change in seawater chemistry (e.g., calcium carbonate saturation state, Iryu & Yamada, 1999; increased Mg/Ca from a calcite sea (Calcite II) to an aragonite sea (Aragonite III) (Stanley, 2006).

Geologic age of the precursor of the dolomitized coral-rich carbonates cannot be directly determined due to absence of age-diagnostic fossil markers and non-dolomitized portions which allow age determinations by Sr isotope stratigraphy. However, we infer that the precursor carbonates were deposited in a coral reef setting during the Oligocene–Miocene based on the abundant occurrence of scleractinian corals and nongeniculate coralline algae.

5.1.1 Rudist and mollusk

Rudist shells occur in molluscan floatstone samples (samples YK17-11C 6K#1502 N4-001 and N5-005). A rudist in the latter sample YK17-11C 6K#1502 N5-005 (Figure 2b) is up to 6.5cm in antero-posterior diameter, and characterized by the presence of a thin (often lost) outer shell layer, the presence of accessory cavities in the posterior and possibly anterior parts of the shell, and the absence of special characters of the shell, such as a celluloprismatic structure in the outer shell layer and pallial canals in the inner shell layer. The combination of these features suggest that it possibly belongs to the primitive form of the Family Caprinulidae, although the lack of the detailed information of their myocardinal arrangements prevents from further taxonomic discussion. The stratigraphic range of non-canaliculate taxa of this family is from the Aptian to the Albian (Steuber et al., 2016). Since rudist specimens in sample YK17-11C 6K#1502 N4-001 are fragmented and preserved in the weathered surface, their identification is uncertain.

Abundant *Chondrodonta* shells occur in the molluscan floatstone (sample YK17-11C 6K#1502 N4-001; Figure 2a). *Chondrodonta* is an oyster-like bivalve belonging to the family Chondrodontidae, and commonly occurs in the Barremian–Cenomanian rudist limestones in the Tethyan carbonate platforms (e.g. Dhondt & Dieni, 1993; Posenato et al., 2018, 2020). This taxon off Minamitorishima usually occurs as bivalved specimens, which are up to 9 cm in size, and is composed of a calcitic foliated outer shell layer and a recrystallized, possibly originally aragonitic inner shell layer. The diagnostic character of this genus, chondrophore (interlocking structure) inside the shell, is observed in one specimen (Figure 9).

5.1.2 Orbitolinid foraminifers

The studied orbitolinid specimens are flat, low conical in shape with an apically situated embryo subdivided into a protoconch, a deuteroconch and a subembryonic zone (Figure 10a–e). These characters distinguish the genus *Mesorbitolina* Schroeder, 1962 (e.g., Loeblich & Tappan, 1987). Deuteroconch and subembryonic zone, more or less equal in thickness, are subdivided by vertical exoskeletal beams (Figure 10b,c). This embryonic apparatus resembles those of *Mesorbitolina parva* (Douglass, 1960) and *Mesorbitolina texana* (Roemer, 1849). These species differ each other in characters occurring in the upper part of the subembryonic zone (e.g., Schlagintweit & Wilsen, 2014). A reliable distinction needs transversal sections of the subembryonic zone (Schroeder, 1975), which are missing in the studied specimens. For this reason, we refer our specimens as to *Mesorbitolina* ex gr. *texana* (Schlagintweit & Wilsen, 2014). Some specimens show exoskeletal and endoskeletal features comparable to *Mesorbitolina birmanica* (Sahni, 1937) (Figure 10e). However, no embryonic apparati of these specimens were recorded.

Based on the stratigraphic range of *M.* ex gr. *texana* (Schroeder et al., 2010), the studied mollusk-rich carbonates are referred to/dated as late Aptian–early Albian. In the studied samples the co-occurrence of *M.* cf. *birmanica* confirms this stratigraphic range (Schlagintweit and Wilsen, 2014; Boudagher-Fadel et al., 2017).

In the Northwest Pacific orbitolinids occurred from the Late Hauterivian to the late Early Albian (Iba et al., 2011). The Tethyan *M.* ex gr. *texana* and *M. birmanica* disappeared at the early–middle Albian boundary (Schroeder et al. 2010; Schlagintweit & Wilsen, 2014) as in the Northwest Pacific area (Iba & Sano, 2008).

5.2 Depositional history

The oceanic crust around Minamitorishima is 160–150 Ma in age (Koppers et al., 2003). The Cretaceous mollusk-rich carbonates collected off this island (~122–111 Ma) is 30–50 Myr younger than the oceanic crust. This indicates that the volcanic edifice of this islands was constructed by an intraplate volcanism between 160–150 Ma and 120–110 Ma.

The dominant components of the studied Cretaceous carbonates are mollusks (including rudists). Corals and calcareous algae are subordinate. These is a common feature known from those on other seamounts (Premoli Silva et al., 1993; Sager et al., 1993). It is known that morphology of mid-Cretaceous carbonate platforms were very unlike Neogene Pacific atolls. Instead of a wave-resistant reef at sea level, the mid-Cretaceous oceanic platform had a submerged platform edge, at a depth of about 30 m, with sponge reefs near the edge, and probably with rudist and coral communities on the uppermost slopes near the edge (Shipboard Science Party, 1993). The occurrence of hermatypic corals (although common) and absence of dasycladalean algae suggest the studied rocks are probably derived from uppermost slopes.

There is a large time gap between the Cretaceous mollusk-rich carbonates and the dolomitized coral-rich carbonates whose precursor was formed in the Oligocene–Miocene. This time gap is not likely to actually exist and caused by a limited number of samples. This interpretation indicates that reefs/carbonate platforms were continuously for the last ~122–111 Myr, filling accommodation space cause by thermal subsidence of Minami-torsi-shima. However, the record of the Cretaceous mollusk-rich carbonates at 938 m and 1085 m water depth provide negative evidence to this interpretation. Assuming that this island has been experienced thermal subsidence since it was formed at 150 Ma and the Cretaceous mollusk-rich carbonates were deposited near the sea-level at 110 Ma, the carbonates should be located at ~2,000 m water depth or deeper at present if we follow the relationship commonly considered to represent standard seafloor subsidence (Parsons & Sclater, 1977). This clearly indicates that Minamitorishima has undergone not continuous thermal subsidence but significant episodic uplifts. Hirano et al. (this issue) reported two stages of Eocene (~40 Ma and ~37 Ma) volcanism occurred at Minamitorishima. This volcanism is likely to have caused thermal rejuvenation of the volcanic edifice of this island and its adjacent oceanic crust and the subsequent uplifts, which is one possible answers to the question why only Mimamitorishima exists as an island. But this remains unsolved.

The coral-rich carbonates were formed in coral reefs as indicated by abundant occurrence of scleractinian hermatypic corals and nongeniculate coralline algae. Abundance of dasycladalean algae in the packstone matrix of two coral floatstone samples (YK17-11C 6K#1502 N5-004 and N5-009) indicates deposition in a shallow protected lagoon environment (Ohba et al., 2017). It is evident that, due to the Eocene uplifts, Minamitorishima was not drowned and coral reefs were extended during a certain period(s) in the Oligocene to Miocene in this island.

Although preservation of the depositional fabrics are various, extensive dissolution are common in the Mimami-tori-shima dolomites. Dissolution vugs and molds of bioclasts are filled partly to completely with crystalline dolomite cement. This occurrence of dolomites indicate that the precursor carbonates were subject to episodic meteoric diagenesis prior to dolomitization. It is shown that geochemical attributes of post-depositional island dolomites are Ca enrichment, positive $\delta^{18}O$ and $\delta^{13}C$, low Sr contents (150–300 ppm) and low Fe (< 300 ppm) and Mn (< 35 ppm) concentrations (Budd, 1997). Six of the seven Minamitorishima dolomites meet these attributes except for one sample (YK17-11C 6K#1502 N5-007). There is no mineral peculiar to a hypersaline setting (e.g., evaporites such as halite and gypsum) and sedimentary structure formed in an evaporitic environment (e.g., desiccation cracks) in any dolomite sample. Consequently, normal seawater is the likely parent fluid of the Minamitorishima dolomites. The post-dolomitization depositional history cannot be reconstructed. The Minamitorishima dolomites have relatively high $\delta^{13}C$ values compared with other post-depositional island dolomites (Budd, 1997). The reason for the high $\delta^{13}C$ values is uncertain at present.

Our study shows that the carbonate deposits at Minamitorishima are potentially ideal source of information on secular evolution of reef/carbonate platform biota for the last ~120 Myr and on tectonic and depositional history of atolls, the volcanic edifice has undergone multiple volcanism. Consequently, deep scientific drilling is expected to be conducted on Minamitorishima in the future.

6. CONCLUSIONS

Minamitorishima is a carbonate island located near the western margin of the Pacific Plate. The oceanic crust around this island formed at 160–150 Ma represents the one of the oldest portions of the Pacific Plate. We performed sedimentological, geochemical and chronological analyses of 19 carbonate rock samples collected from the submarine slope to the west of Minamitorishima by the submersible *Shinkai 6500* during the scientific cruise of *R/V Yokosuka* (YK10-05 and YK17-11C). The collected carbonate rocks were grouped into mollusk-rich carbonates, coral-rich carbonates, foraminiferal-nannofossil packstone, and mudstone and wackestone.

The mollusk-rich carbonates are characterized by the dominance of mollusks (including rudists) and bioeroded bioclasts. Corals and calcareous algae occur as subordinate components. Although plural numerical ages can be assigned for the $^{87}Sr/^{86}Sr$ values of the all shallow-water carbonates, they are determined to be ~122–111 Ma by the occurrence of an age-diagnostic large benthic foraminiferal taxon, *Mesorbitolina* ex gr. *texana*.

The coral-rich carbonates are distinguished by abundance of scleractinian corals and nongeniculate coralline algae associated with encrusting acervulinid foraminifers. This compositional feature is common in shallow-water carbonates formed in the Oligocene onwards (OP-type of Takayanagi et al., 2012). $^{87}Sr/^{86}Sr$ values indicate that the dolomitization occurred at 6.8–9.5 Ma (Tortonian–Messinian). $\delta^{13}C$ and $\delta^{18}O$ values and minor element concentrations shows that normal seawater is the likely parent fluid of the Minamitorishima dolomites.

Foraminiferal-nannofossil packstone (semi-consolidated foraminiferal-nannofossil ooze) is deposited during the period of 0.99–0.45 Ma. Mudstone/wackestone is very poor in fossils and phosphatized; its age and depositional environment are unidentified.

If we assume continuous thermal subsidence since the formation of volcanic edifice of Minamitorishima at ~150 Ma and deposition of the shallow-water carbonates near the sea-level at ~110 Ma, the carbonate should be located at 2000 m water depth or deeper. However, the carbonates were actually recovered at two shallower water depths (938 m and 1085 m), indicating significant episodic uplifts probably by Eocene volcanism (Hirano et al., this issue).

ACKNOWLEDGEMENTS

We thank Mr. Y. Ito and Mr. M. Abe for preparing polished slabs and thin sections of the carbonates collected off Minamitorishima.

REFERENCES

Asahara, Y., Ishiguro, H., Tanaka, T., Yamamoto, K., Mimura, K., Minami, M., & Yoshida, H. (2006). Application of Sr isotopes to geochemical mapping and provenance analysis: the case of Aichi Prefecture, central Japan. *Applied Geochemistry*, *21*, 419–436.

Asahara, Y., Tanaka, T., Kamioka, H., Nishimura, A., & Yamazaki, T. (1999). Provenance of the north Pacific sediments and process of source material transport as derived from Rb–Sr isotopic systematics. *Chemical Geology*, *158*, 271–291.

BouDagher-Fadel, M. K., Hu, X., Price, G. D., Sun, G., Wang, J. G., & An, W. (2017). Foraminiferal biostratigraphy and palaeoenvironmental analysis of the mid-Cretaceous limestones in the southern Tibetan plateau. *Journal of Foraminiferal Research*, *47*, 188–207.

Bown, P. R. & Young, J. R. (1998). Techniques. In: P. R. Bown, (Ed.), *Calcareous Nannofossils Biostratigraphy* (pp. 16–28). Dordrecht: Chapman and Hall (Kluwer Academic Publishers).

Bryan, W. A. (1903). A monograph of Marcus Island. *Occasional Paper of Bernice P. Bishop Museum, Honolulu, Hawaii*, *2*, 77–126.

Cook, H. E., Johnson, P. D., Matti, J. C., Zemmels, I. (1975). Methods of sample preparation and X-ray diffraction data analysis, X-ray mineralogy laboratory. In D. E. Hayes, L. A. Frakes, et al. (Eds.), *Initial Report of the Deep Sea Drilling Project, Volume 28* (pp. 999– 1007). Washington, D. C.: U. S. Government Printing Office.

Dhondt, A.V., & Dieni, I. (1993). Non-rudistid bivalves from Late Cretaceous rudist limestones of the NE Italy (Col Dei Schiosi and Lago di S. Croce areas). *Memorie di Scienze Geologiche : già Memorie degli Istituti di geologia e mineralogia dell'Università di Padova*, *45*, 165–241.

Dunham R. J. (1962). Classification of carbonate rocks according to depositional texture. In W. E. Ham (Ed.), *Classification of Carbonate Rocks.* American Association of Petroleum Geologists Memoir 1 (pp. 108–121). Tulsa, Oklahoma: American Association of Petroleum Geologists.

Embry A. F. & Klovan J. E. (1971). A late Devonian reef tract on northeastern Banks Island, Northwest Territories. *Bulletin of Canadian Petroleum Geology*, *19*, 730–781.

Gartner, S. (1969). Correlation of Neogene planktonic foraminifera and calcareous nannofossil zones. *Transactions of the Gulf-Coast Association of Geological Societies*, *19*, 585–599.

Haggerty, J. A., & Silva, I. P. (1995). Comparison of the origin and evolution of Northwest Pacific guyots drilled during Leg 144. In Haggerty, J. A., Silva, I. P., Rack, F. R., & McNutt, M. K. (Eds.), *Proceedings of the Ocean Drilling Program, Scientific Results, Volume 144* (pp. 935–949). College Station, Texas: Ocean Drilling Program.

Hay, W. W., & Beaudry, F. M. (1973). Calcareous nannofossils – Leg 15, Deep Sea Drilling Projet. Edgar, N. T., Saunders, J. B., et al. (Eds), (1973). *Initial Reports of the Deep Sea Drilling Project, Volume 15* (pp. 625–684), Washington: U.S.Government Printing Office.

Hottinger, L. (2006). *Illustrated Glossary of Terms Used in Foraminiferal Research*. Retrieved from http://paleopolis.rediris.es/cg/06/M02/index.html

Iba, Y. & Sano, S. (2006). *Mesorbitolina* (Cretaceous larger foraminifera) from the Yezo Group in Hokkaido, Japan and its stratigraphic and paleobiogeographic significance. *Proceedings of the Japan Academy Series B, 82*, 216–223.

Iba, Y., Sano, S., & Miura T. (2011). Orbitolinid foraminifers in the Northwest Pacific: their taxonomy and stratigraphy. *Micropaleontology, 57*, 163–171.

Iryu, Y., & Yamada, T. (1999). Biogeochemical contrasts between mid-Cretaceous carbonate platforms and Cenozoic reefs. *Island Arc*, *8*, 475–490.

Kamptner, E. (1963). Coccolithineen-Skelettreste aus Tiefseeablagerungen des Pazifischen Ozeans Eine nannopaläontologische Untersuchung. *Annalen des Naturhistorischen Museums in Wien*, *66*, 139–206.

Kiessling, W. (2009) Geologic and biologic controls on the evolution of reefs. *Annual Review of Ecology, Evolution, and Systematics, 40*, 173–192.

Konishi, K., Tanaka, T., & Omura, A. (1985). Radiocarbon Ages of "Exposed Reef" atMinamitorishima (Marcus Island), Central Pacific. *Proceedings of the Japan Academy, Series B*, *61*, 284–287.

Koppers, A. A., Staudigel, H., Pringle, M. S., & Wijbrans, J. R. (2003). Short-lived and discontinuous intraplate volcanism in the South Pacific: Hot spots or extensional volcanism?. *Geochemistry, Geophysics, Geosystems*, *4*. doi: 10.1029/2003GC000533

Larson, R. L. (1991). Latest pulse of earth: evidence for a mid-Cretaceous super plume. *Geology*, *19*, 547–550.

Loeblich, A. R., & Tappan, H. (1987). Foraminiferal genera and their classification. Van Nostrand Reinhold Co, New York, NY, 2 vols, 970 + 212 pp.

Niitsuma, N. (1998). Renewed continental scientific drilling project and geology in the 21st century. *Memoirs of the Geological Society of Japan*, *49*, 199–225.

Okai, T., Suzuki, A., Terashima, S., Inoue, M., Nohara, M., Kawahata, H., & Imai, N. (2004). Collaborative analysis of GSJ/AIST geochemical reference materials JCp-1 (coral) and JCt-1 (giant clam). *Chikyukagaku (Geochemistry)*, *38*, 281–286. In Japanese with English abstract.

Ohba, H., Matsuda, S., Asami, R., & Iryu, Y. (2017). Recent Dasycladales (Chlorophyta) in Okinawa Jima in the Central Ryukyus, southwestern Japan: Paleontological implications. *Island Arc*, *26*(3), e12185.

Perrin, C. (2002). Tertiary: the emergence of modern reef ecosystems. In Kiessling, W., Flügel, E., & Golonka J. (Eds), *Phanerozoic Reef Patterns*. SEPM Special Publication Number 72 (pp. 587–621). Tulsa, OK: SEPM, Society for Sedimentary Geology.

Posenato, R., Morsilli, M., Guerzoni, S., & Bassi, D. (2018). Palaeoecology of *Chondrodonta* (Bivalvia) from the lower Aptian (Cretaceous) Apulia Carbonate Platform (Gargano Promontory, southern Italy). *Palaeogeography, Palaeoclimatology, Palaeoecology*, *508*, 188–201.

Posenato, R., Frijia, G., Morsilli, M., Moro, A., Del Viscio, G., & Mezga, A. (2020). Paleoecology and proliferation of the bivalve *Chondrodonta joannae* (Choffat) in the upper Cenomanian (Upper Cretaceous) Adriatic Carbonate Platform of Istria (Croatia). *Palaeogeography, Palaeoclimatology, Palaeoecology*, Article 109703. doi: 10.1016/j.palaeo.2020.109703

Premoli Silva, I., Haggerty, J., Rack, F., et al., (1993) *Proceedings of the Ocean Drilling Program, Initial Reports, Volume 144*. College Station, Texas: Ocean Drilling Program.

Roemer, F. (1849). *Texas, mit besonderer rücksicht auf deutsche auswanderung und die physischen verhältnisse des landes nach eigener beobachtung geschildert; mit einem* *naturwissenschaftlichen anhange und einer topographisch–geognistischen karte von Texas*. Bonn: Adolph Marcus.

Sager, W. W., Duncan, R.A., & Handschumacher, D.W. (1993). Paleomagnetism of the Japanese and Marcus-Wake seamounts, western Pacific ocean. In M. S. Pringle, W. W. Sager, W. V. Sliter, & S. Stein (Eds.), *The Mesozoic Pacific: Geology, Tectonics, and Volcanism*. AGU Geophysical Monograph Volume 77 (pp. 401–435). Washington D. C: American Geophysical Union.

Sager, W. W., Winterer, E. L., Firth, J. V., et al., (1993) *Proceedings of the Ocean Drilling Program, Initial Reports, Volume 143*. College Station, Texas: Ocean Drilling Program.

Sahni, M. R. (1937). Discovery of *Orbitolina*-bearing rocks in Burma; with a description of *Orbitolina birmanica* sp. nov. *Records of the Geological Survey of India*, *71*, 360–375.

Sato, T., Chiyonobu, S., & Hodell, D. A. (2009). Data report: Quaternary calcareous nannofossil datums and biochronology in the North Atlantic Ocean, IODP Site U1308. In J. E. T. Channell, T. Kanamatsu, T. Sato, R. Stein, C. A. Alvarez Zarikian, M. J. Malone, & the Expedition 303/306 Scientists (Eds.), Proceedings of the Integrated Ocean Drilling Program, Volume 303/306. Washington, D. C.: Integrated Ocean Drilling Program Management International, Inc. doi:10.2204/iodp.proc.303306.210.2009.

Schlagintweit, F., & Wilsen, M. (2014). Orbitolinid biostratigraphy of the top Taft Formation (Lower Cretaceous of the Yazd Block, Central Iran). *Cretaceous Research, 49*, 125–133.

Schroeder, R. (1975). General evolutionary trends in Orbitolinas. *Revista Española de Micropaleontología, número especial,* 117–128.

Schroeder, R., Van Buchem, F. S. P., Cherchi, A., Baghbani, D., Vincent, B., Immenhauser, A., & Granier, B., (2010). Revised orbitolinid biostratigraphic zonation for the Barremian–Aptian of the eastern Arabian Plate and implications for regional stratigraphic correlations. *GeoArabia Special Publication 4*, 49–96.

Shipboard Scientific Party, 1993. 2. Synthesis of Results. In Sager, W.W., Winterer, E.L., Firth, J.V., et al., *Proceedings of the Ocean Drilling Program, Initial Reports, Volume 143* (pp. 13–29). College Station, Texas: Ocean Drilling Program.

Smoot, N. C. (1989). The Marcus-Wake seamounts and guyots as paleofracture indicators and their relation to the Dutton Ridge. *Marine geology*, *88*, 117–131.

Stanley, S. M. (2006). Influence of seawater chemistry on biomineralization throughout phanerozoic time: paleontological and experimental evidence. *Palaeogeography, Palaeoclimatology, Palaeoecology*, *144*, 3–19.

Steuber, T., Scott, R. W., Mitchell, S. F., & Skelton, P. W. (2016). *Treatise Online no. 81: Part N, Revised, Volume 1, Chapter 26C: Stratigraphy and Diversity Dynamics of Jurassic–Cretaceous Hippuritida (Rudist Bivalves)*. doi: 10.17161/to.v0i0.6474

Suzuki, K., Asahara, Y., Mimura, K., & Tanaka, T. (2012). Another sea area separated from the Panthalassic Ocean in the Norian, the Late Triassic: The lowest Sr isotopic composition of the Ishimaki limestone in central Japan, *Chemie der Erde*, *72*, 77–84.

Suzuki Y., Iryu Y., Inagaki S., Yamada T., Aizawa S., & Budd D. A. (2006). Origin of atoll dolomites distinguished by geochemistry and crystal chemistry: Kita-daito-jima, northern Philippine Sea. *Sedimentary Geology*, *183*, 181–202.

Takayanagi, H., Iryu, Y., Oda, M., Sato, T., Chiyonobu, S., Nishimura, A., Nakazawa, T., Ishikawa, T., & Nagaishi, K. (2012) Temporal changes in biotic and abiotic composition of shallow-water carbonates on submerged seamounts in the northwestern Pacific Ocean and their controlling factors. *Geodiversitas*, *34*, 189–217.

Takayanagi H., Iryu Y., Yamada T., Oda M., Yamamoto K., Sato T., Chiyonobu S., Nishimura A., Nakazawa T., & Shiokawa S. (2007). Carbonate deposits on submerged seamounts in the northwestern Pacific Ocean. *Island Arc*, *16*, 394–419.

Tokuyama, H. (1980). Cretaceous volcanism in the central Pacific Ocean. *Journal of Geography (Chigaku Zasshi)*, *89*, 31–49. In Japanese with English abstract.

Tozer, B, Sandwell, D. T., Smith, W. H. F., Olson, C., Beale, J. R., & Wessel, P. (2019). Global bathymetry and topography at 15 arc sec: SRTM15+. *Earth and Space Science*, 6. Retrieved from https://doi.org/10.1029/2019EA000658

Velic, I. (2007). Stratigraphy and palaeobiogeography of Mesozoic benthic foraminifera of the Karst Dinarides (SE Europe). *Geologia Croatica*, *60*, 1–413.

Table and figure captions

Table 1 List of the shallow-water carbonates collected off Minamitorishima

Table 2 Carbon and oxygen isotope composition and minor element concentrations of the Minamitorishima dolomites

Table 3 $^{87}Sr/^{86}Sr$ values and Sr isotope ages of shallow-water carbonates collected off Minamitorishima. The ages were calculated following the global calibration curve proposed by McArthur et al. (2012). The underline numbers denote the numerical ages that are consistent with rudist biostratigraphy

Figure 1 Maps showing the sample sites.
(a) Geographic location of Minamitorishima; (b) Submarine topography of Minamitorishima showing the localities (Loc. 1, Loc. 2, and Loc. 3) from which the studied carbonate rock samples were retrieved. Bathymetric data retrieved from SRTM15+V2.0 (https://topex.ucsd.edu/WWW_html/srtm15_plus.html; Tozer et al., 2019).

Figure 2 Slab surface of the Cretaceous mollusk-rich carbonates collected off Minamitorishima.
(a) Molluscan floatstone with chondrodont bivalves (YK17-11C 6K#1502 N4-001, 1085 m water depth). (b) Molluscan floatstone (YK17-11C 6K#1502 N5-005; 938 m water depth). (c) Intraclastc-bioclastic rudstone (YK17-11C 6K#1502 N5-006; 938 m water

depth). (d) Molluscan floatstone (YK17-11C 6K#1502 N5-008; 938 m water depth) (e) Carbonate crusts and bioclastic packstone (YK17-11C 6K#1502 N5-010; 938 water depth). (f) Bioclastic grainstone (YK17-11C 6K#1502 N5-011; 938 m water depth). (g) Molluscan rudstone (YK17-11C 6K#1502 N5-014; 938 m water depth). b, bivalve; c, coral; ch, chondrodont bivalve; g, gastropod; r, rudist. Scale bar = 5 cm.

Figure 3 Slab surface of the dolomitized coral-rich carbonates collected off Minamitorishima.

(a) Coral rudstone (YK17-11C 6K#1502 N5-001, 938 m water depth). (b) Fossil coral (YK17-11C 6K#1502 N5-002, 938 m water depth). (c) Coral floatstone (YK17-11C 6K#1502 N5-004, 938 m water depth). (d) Bioclastic grainstone with corals (YK17-11C 6K#1502 N5-007, 938 m water depth). (e) Coral floatstone (YK17-11C 6K#1502 N5-009, 938 m water depth). (f) Fossil coral (YK17-11C 6K#1502 N5-012, 938 m water depth). (g) Coral floatstone (YK17-11C 6K#1502 N5-013, 938 m water depth). (h) Fossil coral (YK17-11C 6K#1502 N5-015, 938 m water depth). a, nongeniculate coralline alga; c. scleractinian coral. Scale bar = 5 cm.

Figure 4 Pleistocene foraminiferal-nannofossil packstone collected off Minamitorishima (YK17-11C 6K#1209 R-05, 3354 m).

Figure 5 Phosphatized mudstone/wackestone collected off Minamitorishima.

(a) Phosphatized mudstone consisting of multiple generations of mudstones (YK17-11C 6K#1502 N4-002, 1085 water depth): i.e., light brown-colored, weakly laminated mudstone (lm), cream- to light brown-colored, porous mudstone (pm), and light brown internal sediment (is). (b) Phosphatized limestone composed of light brown-colored laminated bioclastic wackestone (lw) and dark brown-colored, partly laminated mudstone (lm) (YK17-11C 6K#1502 N5-003, 938 m water depth). Scale bar = 5 cm.

Figure 6 Microfacies of the Cretaceous mollusk-rich carbonates collected off Minamitorishima.

(a) Bioclastic grainstone matrix of molluscan floatstone with chondrodont bivalves (YK17-11C 6K#1502 N4-001, collected at 1085 m water depth), mostly with micrite envelopes. The grainstone is composed mainly medium to coarse sand-sized molluscan shells. (b) The bioclastic grainstone matrix of molluscan floatstone (YK17-11C 6K#1502 N5-005; 938 m water depth). The grainstone consists mainly of fine to medium sand-sized bioclasts of bivalves, gastropods, and intraclasts. Orbitrinid large benthic foraminifers (*Mesorbitolina* cf. *birmanica*) commonly occurs. (c) Intraclastic-bioclastic rudstone (YK17-11C 6K#1502 N5-006; 938 m water depth). Very coarse sand- and granule-sized molluscan shells and intraclasts are abundant. (d) The bioclastic packstone matrix of molluscan floatstone (YK17-11C 6K#1502 N5-008; 938 m water depth). The intergranular granular pore space is filled with peloidal micrite. (e) Carbonate crusts (cc) and bioclastic packstone (YK17-11C 6K#1502 N5-010; 938 water depth). (f) Bioclastic grainstone (YK17-11C 6K#1502 N5-011; 938 m water depth) grainstone composed mainly of coarse sand- and granule-sized bioclasts of mollusks. (g) Bioclastic packstone matrix of molluscan rudstone (YK17-11C 6K#1502 N5-014; 938 m water depth). The packstone consists chiefly of coarse to very coarse sand-sized molluscan shell fragments. The intergranular granular pore space is filled with peloidal micrite. Note traces of bioerosion (arrowed). b, bivalve; cc, carbonate crust; ch, chondrodont; e, echinoid; g, gastropod; i, intraclast; o, orbitolinid large benthic foraminifer, r, rudist. Scale bar = 1 mm.

Figure 7 Microfacies of the dolomitized coral-rich carbonates collected off Minamitorishima.

(a) Coral rudstone (YK17-11C 6K#1502 N5-001, 938 m water depth). Note a coral encrusted by nongeniculate coralline algae and possible grainstone matrix. The nongeniculate coralline algae are selectively preserved. (b) Fossil coral (YK17-11C 6K#1502 N5-002, 938 m water depth). Although skeletal structure of this coral is preserved, the skeleton is replaced with dolomite crystals. (c) Bioclastic packstone matrix of coral floatstone (YK17-11C 6K#1502 N5-004, 938 m water depth). The packstone is dominated by bioclasts of corals, dasycladalean algae, geniculate and nongeniculate coralline algae, bivalves, and gastropods. (d) Bioclastic grainstone (YK17-11C 6K#1502 N5-007, 938 m water depth) with abundant nongeniculate coralline algal grangments.

(e) Bioclastic packstone matrix of the coral floatstone (YK17-11C 6K#1502 N5-009, 938 m water depth). The packstone is composed mainly of bioclasts of corals, nongeniculate coralline algae, mollusks, dasycladalean algae and benthic foraminifers. (f) Coral fragment encrusted by acervulinid foraminifers in the coral floatstone (YK17-11C 6K#1502 N5-009, 938 m water depth). (g) Bioclastic packstone matrix of coral floatstone (YK17-11C 6K#1502 N5-013, 938 m water depth). The bioclasts were dominated by nongeniculate coralline algae due to the selective preservation. (h) Fossil coral (YK17-11C 6K#1502 N5-015, 938 m water depth). Note inter-skeletal pore space filled partly with up to fine sand-sized bioclasts and (partly peloidal) micrite, showing a packstone texture (arrowed). a, nongeniculate coralline alga; b, bivalve; bf, benthic foraminifer; c, coral; d, dasycladalean alga; m, mollusk. Scale bar = 1 mm.

Figure 8 Microfacies of the phosphatized mudstone and wackestone collected off Minamitorishima.

(a) Phosphatized mudstone. Note possible two generations of mudstones (g1 and g2). (b) Phosphatized wackestone and mudstone with abundant, possible molds of microfossils, most of them were dissolved to leave moldic porosity. pf, planktic foraminifer. Scale bar = 1 mm.

Figure 9 A *Chondrodonta* specimen showing an interlocking structure (chondrophore), a diagnostic character of this genus. Sample YK17-11C 6K#1502 N4-001.

ch, chondrophore; il, inter shell layer; ol, outer shell layer. Scale bar = 1 cm.

Figure 10 Orbitolinid foraminifers in the Cretaceous mollusk-rich carbonates collected off Minamitorishima.

(a) Three sub-axial sections of *Mesorbitolina* ex gr. *texana* (Roemer, 1849); sample YK17-11C 6K#1502 N5-010. (b) Enlarged view of the specimen in figure (a) showing the tangential sub-axial section of the embryonic apparatus (c). (d) *Mesorbitolina* ex gr. *texana*, sub-axial section showing the septa and the complex exoskeleton with beams and rafters; sample YK17-11C 6K#1502 N5-005. (e) *Mesorbitolina* cf. *birmanica* (Sahni, 1937), oblique sub-axial section; sample YK17-11C 6K#1502 N5-005. b, beam; d, deuteroconch; e, epiderm; f, foramen; p, protoconch; r, rafter; s, septum; sl, septulum; sz, subembryonic zone. Scale bars are 1 mm in a, d–e, and 0.2 mm in b–c.

Table 1 List of the shallow-water carbonates collected from the submarine slope to the west of Minami-tori-shima

Rock No.	Latitude	Longitude	Water Depth (m)	Rock name	Mineralogy
YK17-11C 6K#1209 R-05	24°21.2415’N	153°53.0887’E	3354	Foraminiferal-nannofossil ooze	Calcite
YK17-11C 6K#1502 N5-001	24°17.5487'N	153°56.3431'E	938	Coral rudstone	Dolomite
YK17-11C 6K#1502 N5-002	24°17.5487'N	153°56.3431'E	938	Fossil coral	Dolomite
YK17-11C 6K#1502 N5-004	24°17.5487'N	153°56.3431'E	938	Coral floatstone	Dolomite
YK17-11C 6K#1502 N5-007	24°17.5487'N	153°56.3431'E	938	Bioclastic grainstone with corals	Dolomite
YK17-11C 6K#1502 N5-009	24°17.5487'N	153°56.3431'E	938	Coral floatstone	Dolomite
YK17-11C 6K#1502 N5-012	24°17.5487'N	153°56.3431'E	938	Fossil coral	Dolomite
YK17-11C 6K#1502 N5-013	24°17.5487'N	153°56.3431'E	938	Coral floatstone	Dolomite
YK17-11C 6K#1502 N5-015	24°17.5487'N	153°56.3431'E	938	Fossil coral	Dolomite
YK17-11C 6K#1502 N4-002	24°17.5522'N	153°56.1794'E	1085	Phosphatized mudstone	Apatite
YK17-11C 6K#1502 N5-003	24°17.5487'N	153°56.3431'E	938	Phosphatized mudstone	Apatite
YK17-11C 6K#1502 N4-001	24°17.5522'N	153°56.1794'E	1085	Molluscan floatstone with chondrodont bivalves	Calcite
YK17-11C 6K#1502 N5-005	24°17.5487'N	153°56.3431'E	938	Molluscan floatstone	Calcite
YK17-11C 6K#1502 N5-006	24°17.5487'N	153°56.3431'E	938	Intraclastic-bioclastic rudstone	Calcite
YK17-11C 6K#1502 N5-008	24°17.5487'N	153°56.3431'E	938	Molluscan floatstone	Calcite
YK17-11C 6K#1502 N5-010	24°17.5487'N	153°56.3431'E	938	Carbonate crusts and bioclastic packstone	Calcite
YK17-11C 6K#1502 N5-011	24°17.5487'N	153°56.3431'E	938	Bioclastic grainstone	Calcite
YK17-11C 6K#1502 N5-014	24°17.5487'N	153°56.3431'E	938	Molluscan rudstone	Calcite

Table 2 Carbon and oxygen isotope composition and minor element concentrations of the Minami-tori-shima dolomites

Rock No.	Rock name	$\delta^{13}C$ ‰ VPDB	$\delta^{18}O$ ‰ VPDB	Mn ppm	Fe ppm	Sr ppm
YK17-11C 6K#1502 N5-001	Coral rudstone	3.65	1.66	27	170	220
		3.85	1.50	28	180	220
		3.96	1.66	28	180	240
YK17-11C 6K#1502 N5-002	Fossil coral	3.81	1.54	31	180	200
YK17-11C 6K#1502 N5-007	Bioclastic grainstone with corals	3.64	1.77	120	170	220
		3.77	1.51	34	170	250
YK17-11C 6K#1502 N5-012	Fossil coral	4.07	1.88	27	190	230

Table 3 $^{87}Sr/^{86}Sr$ values and Sr isotope ages of shallow-water carbonates collected off Minami-tori-shima. The ages were calculated following the global calibration curve proposed by McArthur et al. (2012) . The underline numbers denote the numerical ages that are consistent with large bethic foraminiferal biostratigraphy

Rock No.	Rock Name	Mineral	$^{87}Sr/^{86}Sr$	2SE	Age (Ma)			Range	Geologic Time
					Oldest	Mean	Youngest	(Myr)	
YK17-11C 6K#1209 R-05	Foraminifer-nannofossil ooze	Calcite							
YK17-11C 6K#1502 N5-001	Coral rudstone	Dolomite	0.708929	±0.000018	9.3	8.2	7.0	2.3	Miocene (Tortonian)
			0.708914	±0.000018	9.8	9.0	7.7	2.1	Miocene (Tortonian)
			0.708908	±0.000020	10.0	9.2	7.9	2.1	Miocene (Tortonian)
YK17-11C 6K#1502 N5-002	Fossil coral	Dolomite	0.708918	±0.000020	9.7	8.8	7.3	2.4	Miocene (Tortonian)
YK17-11C 6K#1502 N5-004	Coral floatstone	Dolomite	0.708934	±0.000013	8.9	7.8	7.0	1.9	Miocene (Tortonian)
YK17-11C 6K#1502 N5-007	Bioclastic grainstone with coralss	Dolomite	0.708909	±0.000018	9.9	9.2	8.0	1.9	Miocene (Tortonian)
			0.708920	±0.000018	9.6	8.7	7.3	2.2	Miocene (Tortonian)
YK17-11C 6K#1502 N5-009	Coral floatstone	Dolomite	0.708940	±0.000013	8.5	7.4	6.8	1.7	Miocene (Tortonian)
YK17-11C 6K#1502 N5-012	Fossil coral	Dolomite	0.708956	±0.000014	7.6	6.8	6.3	1.2	Miocene (Messinian)
YK17-11C 6K#1502 N5-013	Coral floatstone	Dolomite	0.708901	±0.000014	10.1	9.5	8.7	1.4	Miocene (Tortonian)
YK17-11C 6K#1502 N5-015	Fossil coral	Dolomite	0.708903	±0.000014	10.0	9.4	8.6	1.4	Miocene (Tortonian)
YK17-11C 6K#1502 N4-001	Molluscan floatstone with chondrodont bivalves	Calcite	0.707272	±0.000011	113.7	113.2	112.8	0.9	Aptian
					119.5	118.3	117.1	2.4	Aptian
					141.2	140.4	139.7	1.5	Berriasian
YK17-11C 6K#1502 N5-005	Molluscan floatstone	Calcite	0.707286	±0.000014	113.5	113.0	112.4	1.0	Albian
					120.4	119.2	117.6	2.8	Aptian
					140.6	139.7	138.9	1.7	Berriasian
YK17-11C 6K#1502 N5-006	Intraclastic-bioclastic rudstone	Calcite	0.707310	±0.000014	90.3	89.9	89.4	0.9	Turonian
					92.7	92.0	90.8	1.9	Turonian
					112.9	112.4	111.8	1.1	Albian
					121.9	120.7	119.1	2.7	Aptian
					139.4	138.6	137.8	1.6	Valanginian
YK17-11C 6K#1502 N5-008	Molluscan floatstone with rudists	Calcite	0.707223	±0.000014	115.1	114.2	113.7	1.5	Aptian
					117.1	116.2	115.1	2.0	Aptian
					143.9	143.0	142.0	1.9	Berriasian
YK17-11C 6K#1502 N5-010	Carbonate crusts and bioclastic packstone	Calcite	0.707333	±0.000013	89.8	89.3	88.7	1.1	Coniacian
					93.4	92.8	92.2	1.2	Turonian
					112.3	111.8	111.2	1.1	Albian
					123.2	122.2	121.2	2.0	Aptian
					138.4	137.7	136.8	1.6	Valanginian
YK17-11C 6K#1502 N5-011	Bioclastic grainstone	Calcite	0.707239	±0.000014	114.4	113.9	113.4	1.0	Aptian
					117.9	116.7	115.9	2.0	Aptian
					143.2	142.2	141.2	2.0	Berriasian
YK17-11C 6K#1502 N5-014	Molluscan rudstone	Calcite	0.707357	±0.000013	89.1	88.5	87.9	1.2	Coniacian
					94.3	93.6	93.0	1.3	Turonian
					111.7	111.1	110.4	1.4	Albian
					124.2	123.6	122.7	1.5	Aptian
					137.4	136.4	134.6	2.8	Valanginian

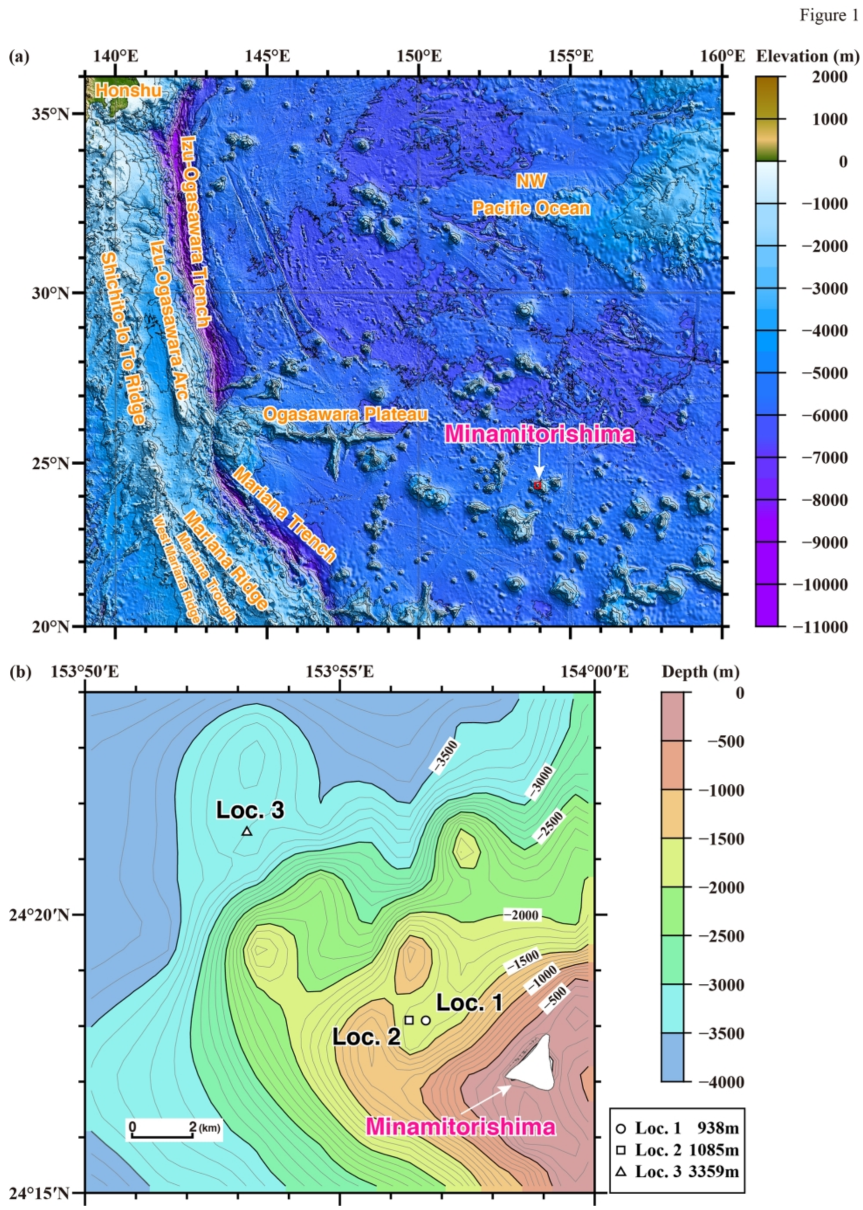

Figure 1 Maps showing the sample sites.
(a) Geographic location of Minamitorishima; (b) Submarine topography of Minamitorishima showing the localities (Loc. 1, Loc. 2, and Loc. 3) from which the studied carbonate rock samples were retrieved. Bathymetric data retrieved from SRTM15+V2.0 (https://topex.ucsd.edu/WWW_html/srtm15_plus.html; Tozer et al., 2019).

165x232mm (300 x 300 DPI)

Figure 2

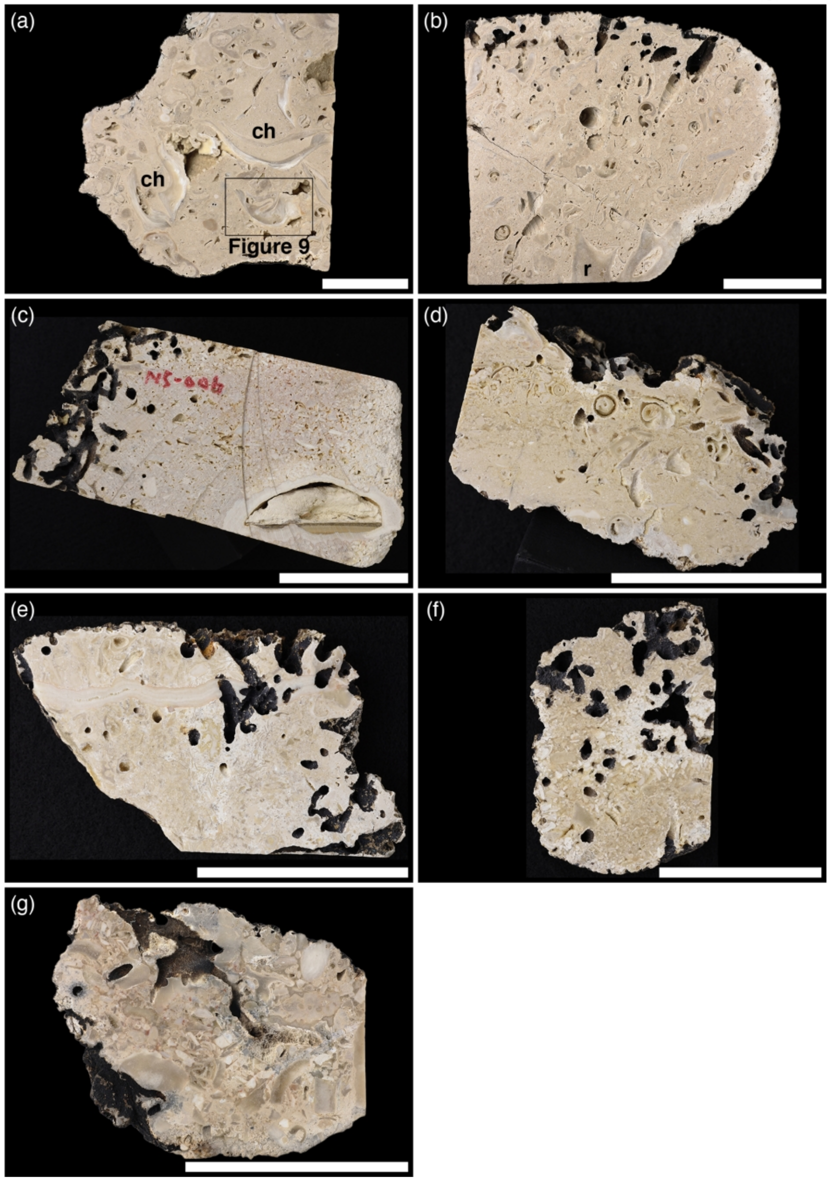

Figure 2 Slab surface of the Cretaceous mollusk-rich carbonates collected off Minamitorishima. (a) Molluscan floatstone with chondrodont bivalves (YK17-11C 6K#1502 N4-001, 1085 m water depth). (b) Molluscan floatstone (YK17-11C 6K#1502 N5-005; 938 m water depth). (c) Intraclastc-bioclastic rudstone (YK17-11C 6K#1502 N5-006; 938 m water depth). (d) Molluscan floatstone (YK17-11C 6K#1502 N5-008; 938 m water depth) (e) Carbonate crusts and bioclastic packstone (YK17-11C 6K#1502 N5-010; 938 water depth). (f) Bioclastic grainstone (YK17-11C 6K#1502 N5-011; 938 m water depth). (g) Molluscan rudstone (YK17-11C 6K#1502 N5-014; 938 m water depth). b, bivalve; c, coral; ch, chondrodont bivalve; g, gastropod; r, rudist. Scale bar = 5 cm.

165x240mm (300 x 300 DPI)

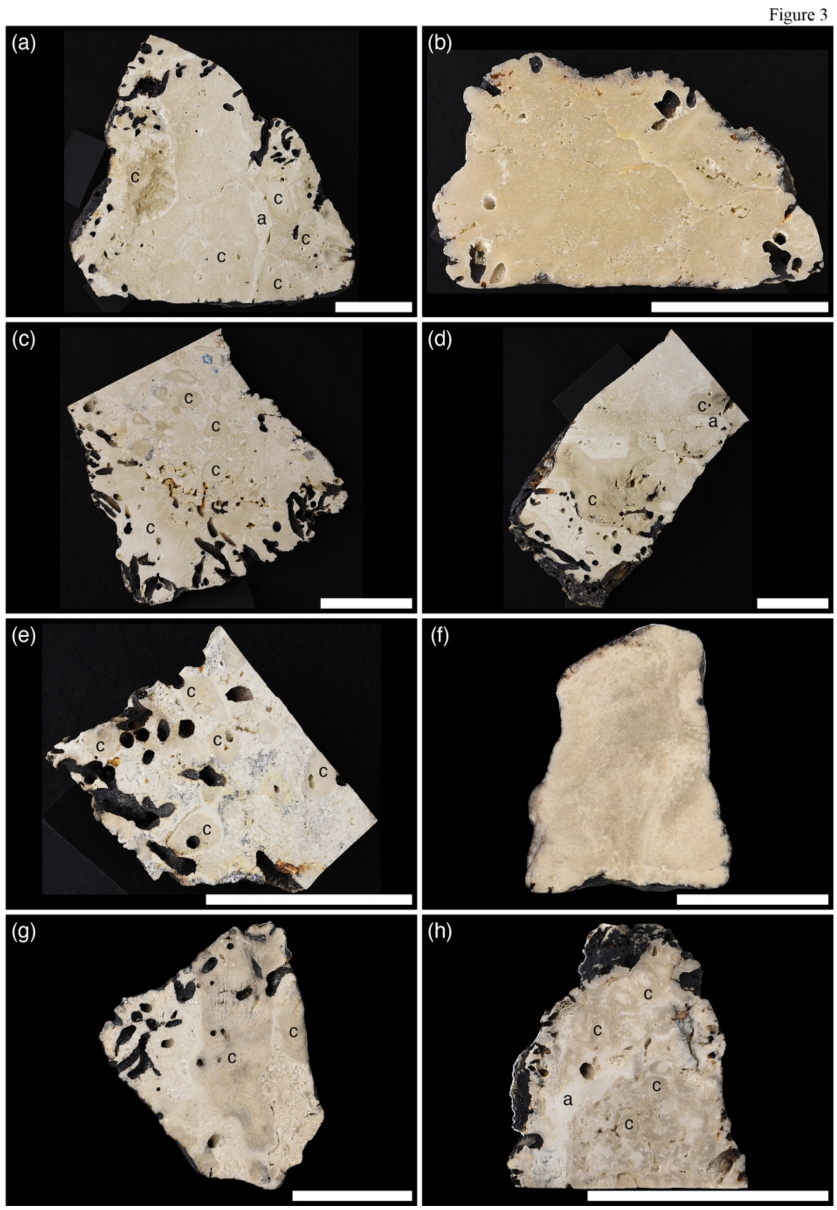

Figure 3 Slab surface of the dolomitized coral-rich carbonates collected off Minamitorishima. (a) Coral rudstone (YK17-11C 6K#1502 N5-001, 938 m water depth). (b) Fossil coral (YK17-11C 6K#1502 N5-002, 938 m water depth). (c) Coral floatstone (YK17-11C 6K#1502 N5-004, 938 m water depth). (d) Bioclastic grainstone with corals (YK17-11C 6K#1502 N5-007, 938 m water depth). (e) Coral floatstone (YK17-11C 6K#1502 N5-009, 938 m water depth). (f) Fossil coral (YK17-11C 6K#1502 N5-012, 938 m water depth). (g) Coral floatstone (YK17-11C 6K#1502 N5-013, 938 m water depth). (h) Fossil coral (YK17-11C 6K#1502 N5-015, 938 m water depth). a, nongeniculate coralline alga; c. scleractinian coral. Scale bar = 5 cm.

165x238mm (300 x 300 DPI)

Figure 4

Figure 4 Pleistocene foraminiferal-nannofossil packstone collected off Minamitorishima.

85x67mm (300 x 300 DPI)

Figure 5

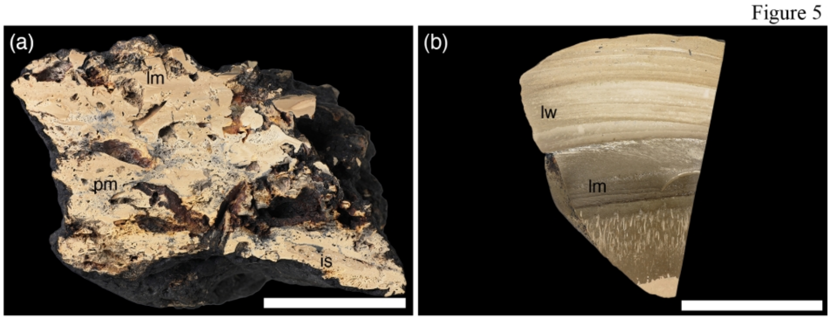

Figure 5 Phosphatized mudstone/wackestone collected off Minamitorishima.
(a) Phosphatized mudstone consisting of multiple generations of mudstones (YK17-11C 6K#1502 N4-002, 1085 water depth): i.e., light brown-colored, weakly laminated mudstone (lm), cream- to light brown-colored, porous mudstone (pm), and light brown internal sediment (is). (b) Phosphatized limestone composed of light brown-colored laminated bioclastic wackestone (lw) and dark brown-colored, partly laminated mudstone (lm) (YK17-11C 6K#1502 N5-003, 938 m water depth). Scale bar = 5 cm.

165x239mm (300 x 300 DPI)

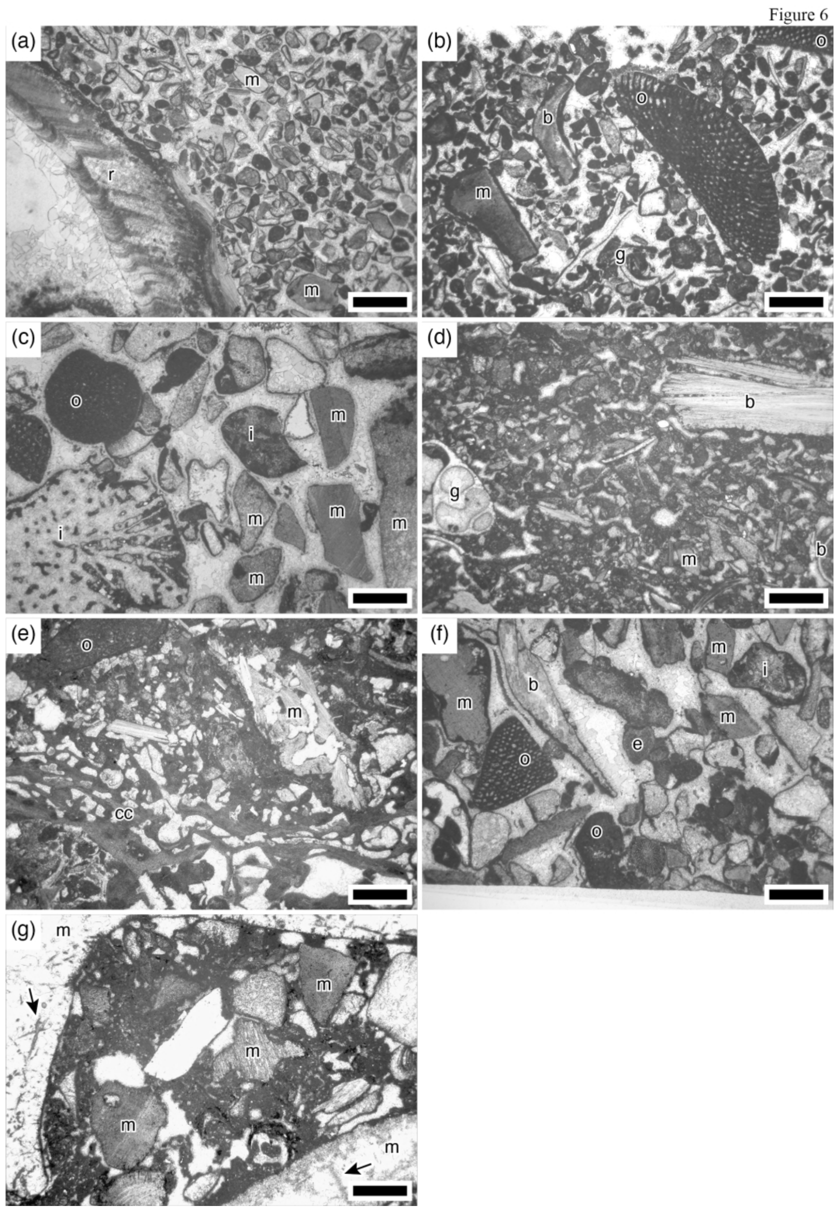

Figure 6 Microfacies of the Cretaceous mollusk-rich carbonates collected off Minamitorishima. (a) Bioclastic grainstone matrix of molluscan floatstone with chondrodont bivalves (YK17-11C 6K#1502 N4-001, collected at 1085 m water depth), mostly with micrite envelopes. The grainstone is composed mainly medium to coarse sand-sized molluscan shells. (b) The bioclastic grainstone matrix of molluscan floatstone (YK17-11C 6K#1502 N5-005; 938 m water depth). The grainstone consists mainly of fine to medium sand-sized bioclasts of bivalves, gastropods, and intraclasts. Orbitrinid large benthic foraminifers (Mesorbitolina cf. birmanica) commonly occurs. (c) Intraclastic-bioclastic rudstone (YK17-11C 6K#1502 N5-006; 938 m water depth). Very coarse sand- and granule-sized molluscan shells and intraclasts are abundant. (d) The bioclastic packstone matrix of molluscan floatstone (YK17-11C 6K#1502 N5-008; 938 m water depth). The intergranular granular pore space is filled with peloidal micrite. (e) Carbonate crusts (cc) and bioclastic packstone (YK17-11C 6K#1502 N5-010; 938 water depth). (f) Bioclastic grainstone (YK17-11C 6K#1502 N5-011; 938 m water depth) grainstone composed mainly of coarse sand- and granule-sized bioclasts of mollusks. (g) Bioclastic packstone matrix of molluscan rudstone (YK17-11C 6K#1502 N5-014; 938 m water depth). The packstone consists chiefly of coarse to very coarse sand-sized molluscan shell fragments. The

intergranular granular pore space is filled with peloidal micrite. Note traces of bioerosion (arrowed). b, bivalve; cc, carbonate crust; ch, chondrodont; e, echinoid; g, gastropod; i, intraclast; o, orbitolinid large benthic foraminifer, r, rudist. Scale bar = 1 mm.

165x239mm (300 x 300 DPI)

Figure 7

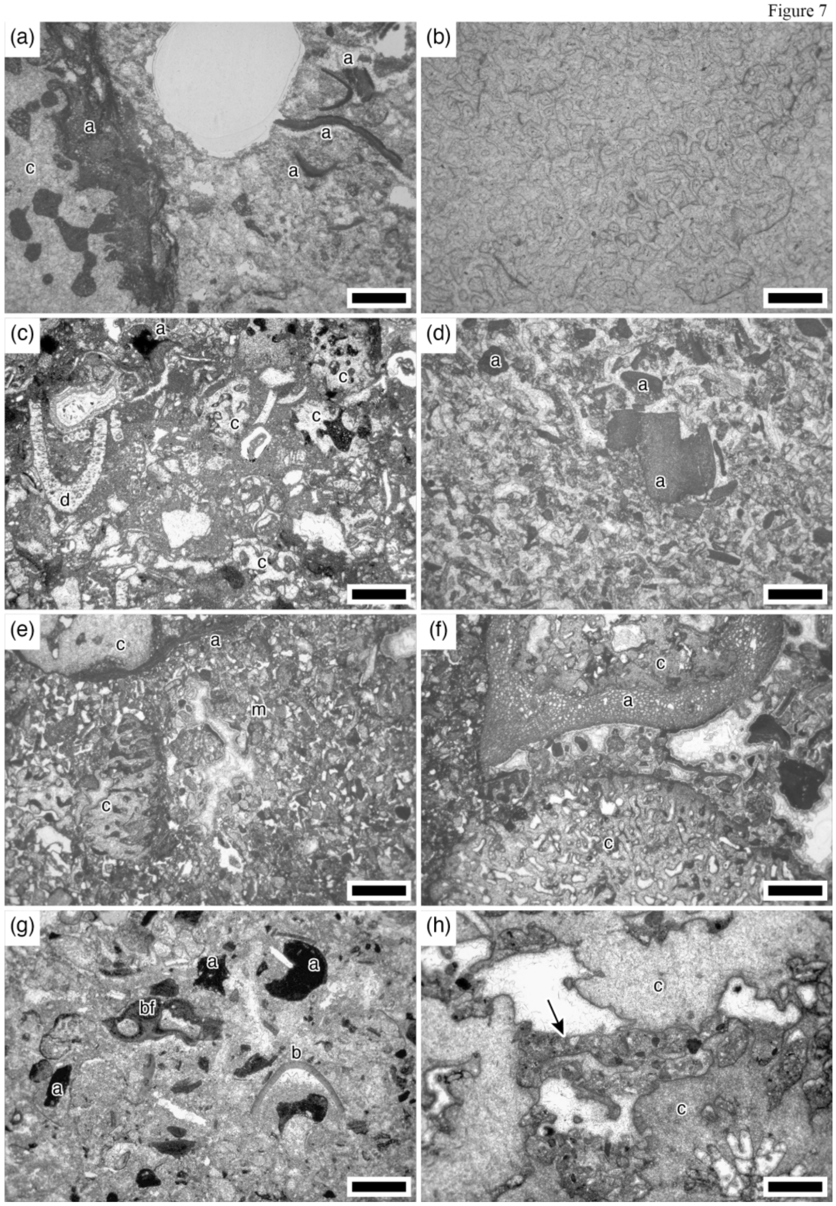

Figure 7 Microfacies of the dolomitized coral-rich carbonates collected off Minamitorishima.
(a) Coral rudstone (YK17-11C 6K#1502 N5-001, 938 m water depth). Note a coral encrusted by nongeniculate coralline algae and possible grainstone matrix. The nongeniculate coralline algae are selectively preserved. (b) Fossil coral (YK17-11C 6K#1502 N5-002, 938 m water depth). Although skeletal structure of this coral is preserved, the skeleton is replaced with dolomite crystals. (c) Bioclastic packstone matrix of coral floatstone (YK17-11C 6K#1502 N5-004, 938 m water depth). The packstone is dominated by bioclasts of corals, dasycladalean algae, geniculate and nongeniculate coralline algae, bivalves, and gastropods. (d) Bioclastic grainstone (YK17-11C 6K#1502 N5-007, 938 m water depth) with abundant nongeniculate coralline algal grangments.
(e) Bioclastic packstone matrix of the coral floatstone (YK17-11C 6K#1502 N5-009, 938 m water depth). The packstone is composed mainly of bioclasts of corals, nongeniculate coralline algae, mollusks, dasycladalean algae and benthic foraminifers. (f) Coral fragment encrusted by acervulinid foraminifers in the coral floatstone (YK17-11C 6K#1502 N5-009, 938 m water depth). (g) Bioclastic packstone matrix of coral floatstone (YK17-11C 6K#1502 N5-013, 938 m water depth). The bioclasts were dominated by

nongeniculate coralline algae due to the selective preservation. (h) Fossil coral (YK17-11C 6K#1502 N5-015, 938 m water depth). Note inter-skeletal pore space filled partly with up to fine sand-sized bioclasts and (partly peloidal) micrite, showing a packstone texture (arrowed). a, nongeniculate coralline alga; b, bivalve; bf, benthic foraminifer; c, coral; d, dasycladalean alga; m, mollusk. Scale bar = 1 mm.

165x239mm (300 x 300 DPI)

Figure 8

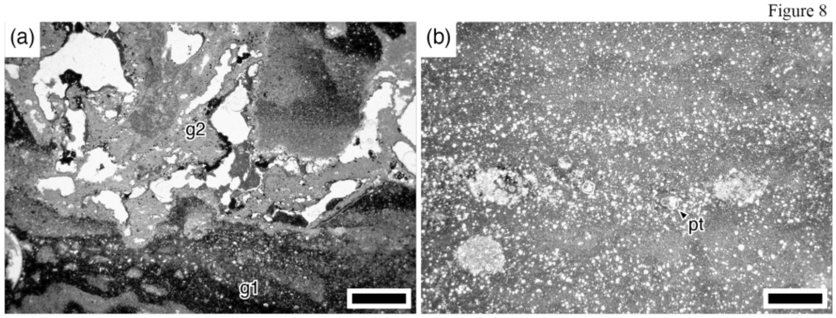

Figure 8 Microfacies of the phosphatized mudstone and wackestone collected off Minamitorishima. (a) Phosphatized mudstone. Note possible two generations of mudstones (g1 and g2). (b) Phosphatized wackestone and mudstone with abundant, possible molds of microfossils, most of them were dissolved to leave moldic porosity. pf, planktic foraminifer. Scale bar = 1 mm.

165x239mm (300 x 300 DPI)

Figure 9

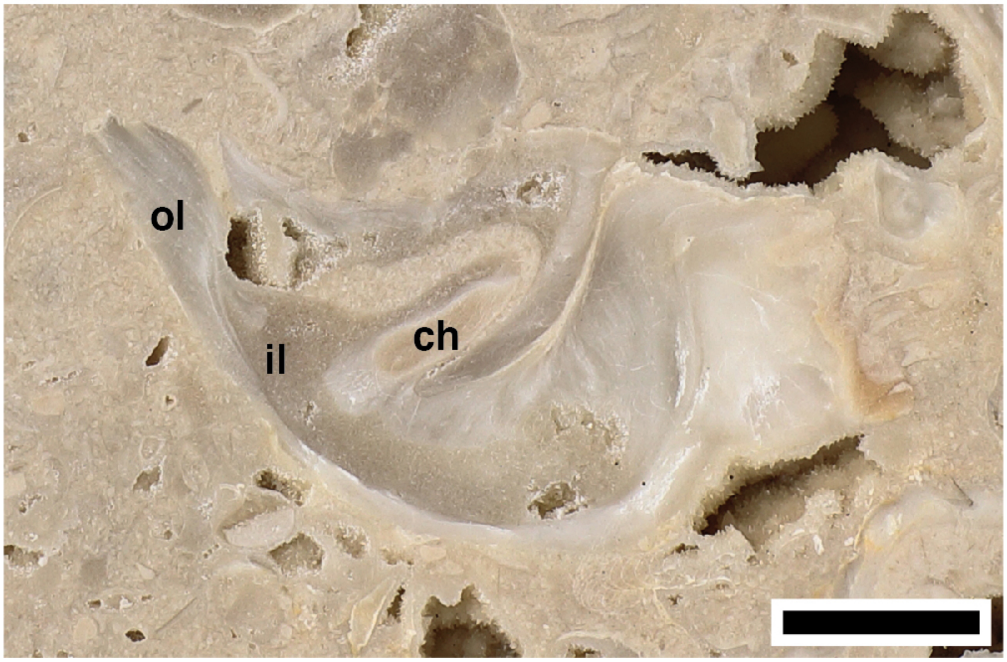

Figure 9 A Chondrodonta specimen showing an interlocking structure (chondrophore), a diagnostic character of this genus. Sample YK17-11C 6K#1502 N4-001.
ch, chondrophore; il, inter shell layer; ol, outer shell layer. Scale bar = 1 cm.

85x60mm (300 x 300 DPI)

Figure 10

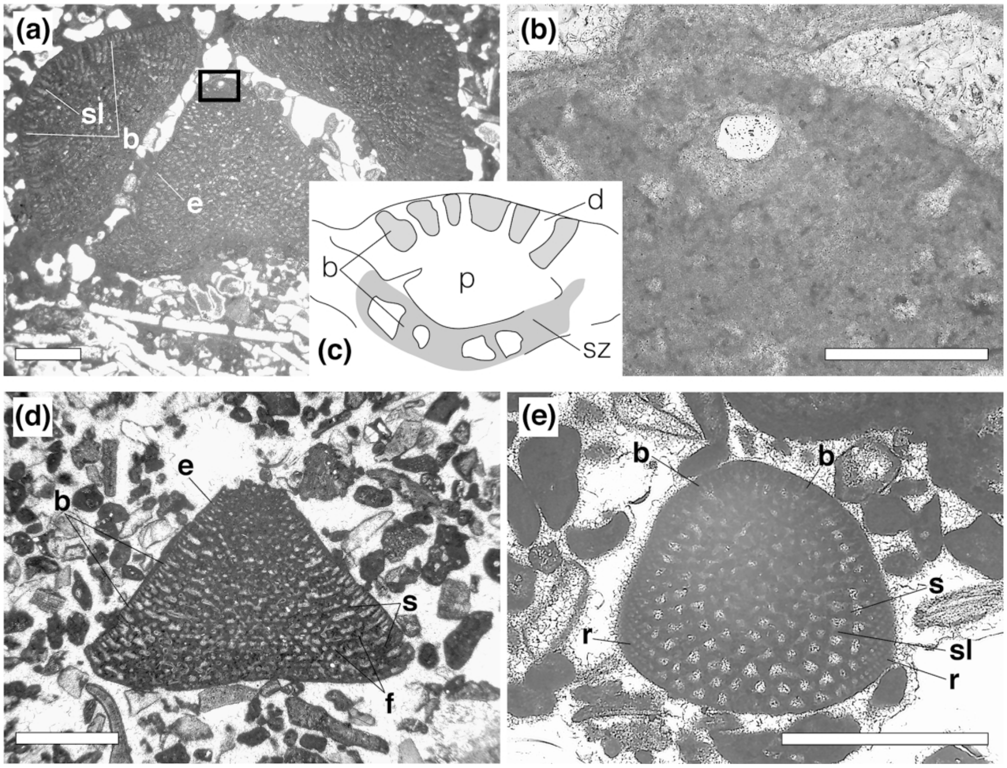

Figure 10 Orbitolinid foraminifers in the Cretaceous mollusk-rich carbonates collected off Minamitorishima. (a) Three sub-axial sections of Mesorbitolina ex gr. texana (Roemer, 1849); sample N5-010. (b) Enlarged view of the specimen in figure (a) showing the tangential sub-axial section of the embryonic apparatus (c). (d) Mesorbitolina ex gr. texana, sub-axial section showing the septa and the complex exoskeleton with beams and rafters; sample N5-005. (e) Mesorbitolina cf. birmanica (Sahni, 1937), oblique sub-axial section; sample N5-005. Scale bars are 1 mm in a, d–e, and 0.2 mm in b–c. b, beam; d, deuteroconch; e, epiderm; f, foramen; p, protoconch; r, rafter; s, septum; sl, septulum; sz, subembryonic zone. Scale bars are 1 mm in a, d–e, and 0.2 mm in b–c.